

Discovery of a Small Molecule MDM2 Inhibitor (AMG 232) for Treating Cancer

Yosup Rew, and Daqing Sun

J. Med. Chem., **Just Accepted Manuscript** • DOI: 10.1021/jm500627s • Publication Date (Web): 26 Jun 2014

Downloaded from <http://pubs.acs.org> on June 30, 2014

Just Accepted

“Just Accepted” manuscripts have been peer-reviewed and accepted for publication. They are posted online prior to technical editing, formatting for publication and author proofing. The American Chemical Society provides “Just Accepted” as a free service to the research community to expedite the dissemination of scientific material as soon as possible after acceptance. “Just Accepted” manuscripts appear in full in PDF format accompanied by an HTML abstract. “Just Accepted” manuscripts have been fully peer reviewed, but should not be considered the official version of record. They are accessible to all readers and citable by the Digital Object Identifier (DOI®). “Just Accepted” is an optional service offered to authors. Therefore, the “Just Accepted” Web site may not include all articles that will be published in the journal. After a manuscript is technically edited and formatted, it will be removed from the “Just Accepted” Web site and published as an ASAP article. Note that technical editing may introduce minor changes to the manuscript text and/or graphics which could affect content, and all legal disclaimers and ethical guidelines that apply to the journal pertain. ACS cannot be held responsible for errors or consequences arising from the use of information contained in these “Just Accepted” manuscripts.



Discovery of a Small Molecule MDM2 Inhibitor (AMG 232) for Treating Cancer

Yosup Rew* and Daqing Sun*

Departments of Therapeutic Discovery, Amgen Inc., 1120 Veterans Boulevard, South San Francisco, California 94080, United States

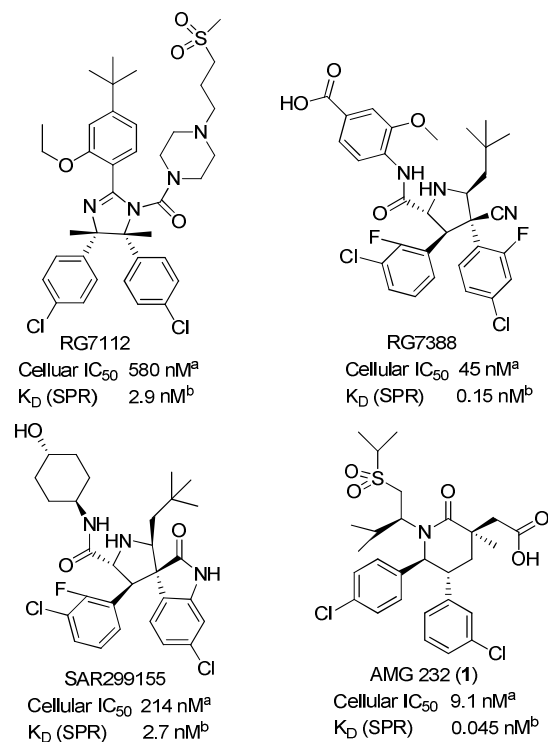
KEYWORDS: MDM2, p53, protein-protein interaction, piperidinone, AMG 232.

ABSTRACT: We recently reported the discovery of AMG 232 (**1**), a potent and selective piperidinone inhibitor of the MDM2-p53 protein-protein interaction. Compound **1** is currently being evaluated in human clinical trials for the treatment of cancer. This article provides an overview of its discovery from the de novo design of the piperidinone series to the structure-activity studies leading to the identification of **1**. In addition, this article also describes the preclinical pharmacology and pharmacokinetics of **1**, along with its drug metabolism and safety assessment.

INTRODUCTION

The p53 tumor suppressor protein induces cell growth arrest and apoptosis in response to DNA damage or stress,¹ and it has been proposed that inactivation of the p53 pathway may be a required step for tumor survival.² Approximately 50% of human cancers have p53 mutations resulting in loss of its function.³ The wild-type p53, present in the remaining 50% of

1
2
3 malignancies, is downregulated by the MDM2 (human murine double minute 2) oncoprotein via
4 a direct protein-protein interaction.^{2,4} After binding to p53, MDM2 inhibits p53 activity by
5 blocking p53 mediated transactivation,⁵ inducing nuclear export of p53,⁶ and acting as E3
6 ubiquitin ligase targeting both itself and p53 for the degradation by the 26S proteasome.⁷ Since
7 all of these mechanisms can be blocked by neutralizing the MDM2-p53 interaction, disruption of
8 the protein-protein interaction with small molecule MDM2 inhibitors has been considered a
9 promising strategy to reactivate the p53 pathway in wild-type p53 tumors over the last two
10 decades.⁸ To date, a couple of studies with small molecule MDM2 inhibitors have demonstrated
11 tumor growth inhibition both in vitro and in vivo,⁹⁻¹¹ and several small molecules have recently
12 advanced into clinical trials (Figure 1).¹²⁻¹⁵
13
14
15
16
17
18
19
20
21
22
23
24
25
26
27
28
29
30
31
32
33
34
35
36
37
38
39
40
41
42
43
44
45
46
47
48
49
50
51
52
53
54
55
56
57
58
59
60



29 **Figure 1.** Chemical structures and potencies of RG7112 (Roche),^{13a} RG7388 (Roche),^{13b}
30 SAR299155 (Sanofi),¹⁴ and **1**.¹⁵ ^aIC₅₀ in the EdU proliferation assay (SJSA-1, 10% human
31 serum); ^bK_D in the surface plasmon resonance (SPR) spectroscopy binding assay.
32
33
34
35
36
37
38
39

40 Recently, we reported the discovery of a promising piperidinone MDM2 inhibitor, **1**
41 (AMG 232),^{11,15} which is currently being evaluated in human clinical trials. In this article, we
42 provide a comprehensive overview of the scientific efforts focused on the discovery of
43 compound **1**: (a) de novo design of piperidinone inhibitors; (b) optimization of piperidinone
44 series inhibitors via conformational controls and extensive SAR; (c) discovery of **1** via capturing
45 an additional interaction with Gly58 shelf region; (d) chemical synthesis of **1**; (e) in vitro and in
46 vivo pharmacology; (f) binding mode; and (g) drug metabolism. Finally, this article briefly
47 describes (h) preclinical pharmacokinetics and human PK prediction, and (i) safety assessment.
48
49
50
51
52
53
54
55
56
57
58
59
60

DE NOVO DESIGN OF PIPERIDINONE INHIBITORS¹¹

Our early research in the MDM2 program focused on the optimization of a class of chromenotriazolopyrimidine inhibitors identified from high throughput screening of a small-molecule library (Amgen, High-throughput screening (HTS) lead; Figure 2).¹⁶ To complement these efforts, we initiated a parallel strategy, a de novo design approach to identify a novel scaffold of MDM2 inhibitors. In 1996, the crystal structure of the p53 binding domain of human MDM2 bound to a 15-residue peptide of human p53 was reported and unveiled that three hydrophobic residues of p53 (Phe19, Trp23, and Leu26) are essential for key hydrophobic contacts with the MDM protein.¹⁷ Subsequently, these key hydrophobic interactions were confirmed by the co-crystal structures of small molecule inhibitors with MDM2 (Figure 2).

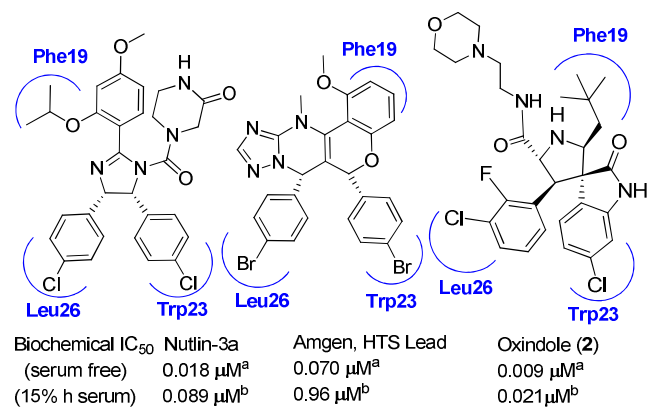


Figure 2. Binding modes of known MDM2 inhibitors, Nutlin-3a,^{9a} Amgen's HTS Lead,^{16a} and Oxindole (2).¹⁸ MDM2 binding pockets are labeled (by p53 side chain) in blue. ^aIC₅₀ in the homogeneous time-resolved fluorescence (HTRF) assay (serum free); ^bIC₅₀ in the HTRF biochemical assay (15% human serum).¹¹

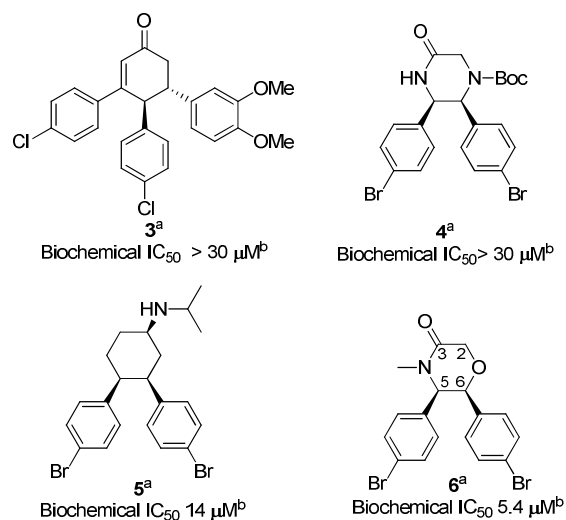


Figure 3. Early hits from de novo design. ^{11b} ^aCompounds are racemic; ^bIC₅₀ in the HTRF biochemical assay (serum free).

Analysis of the binding modes of these known MDM2 inhibitors promoted us to design several new scaffolds based on a common structural element of two aromatic groups held in close proximity by a rigid cyclic core. These efforts resulted in the identification of multiple hits including a morpholinone series, as illustrated by compound **6**, with an IC₅₀ of 5 μM in the HTRF biochemical assay (Figure 3). Adding a benzyl group at the C2 position in **6** improved potency about 2.5-fold (**7** vs. **6** in Figure 4). At a glance, we presumed that three aryl groups of **7** contact the corresponding key binding clefts in the MDM2 protein. However, the co-crystal structure of **7** with MDM2 revealed that only two hydrophobic Trp23_(p53) and Phe19_(p53) pockets are filled by the *p*-bromophenyl rings, respectively and the Leu26_(p53) pocket remains unoccupied (Figure 5a). The benzyl group employs an edge-face aromatic contact with the Phe55 residue on a shallow hydrophobic shelf region.

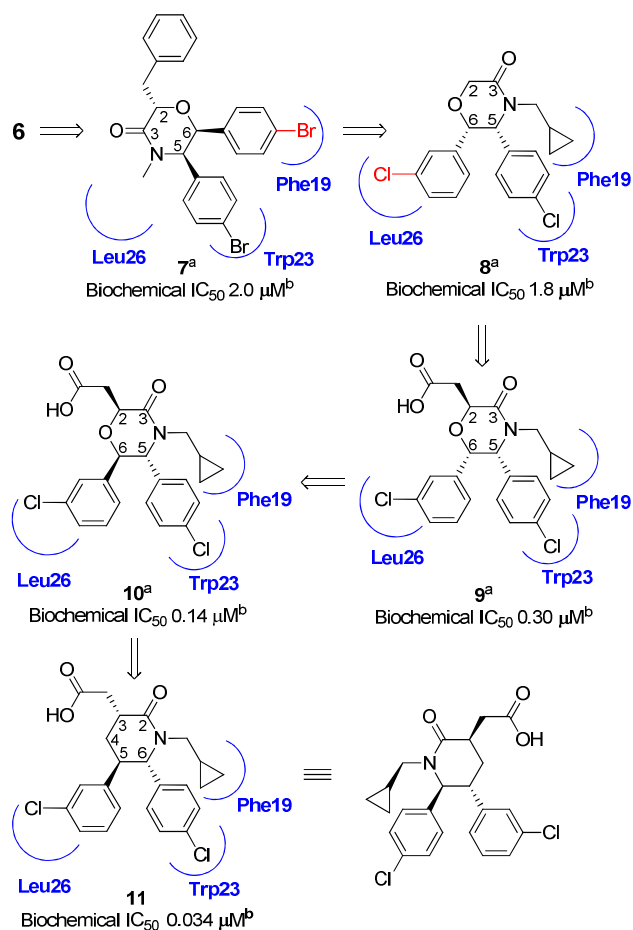
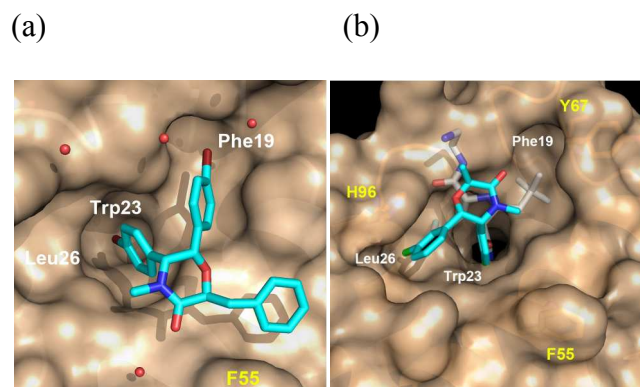


Figure 4. Discovery of the novel piperidinone lead **11** from the early hit **6**.¹¹ MDM2 binding pockets are labeled (by p53 side chain) in blue. ^aCompounds are racemic; ^b IC_{50} in the HTRF biochemical assay (serum free).

As one of the strategies to fill the Leu26_(p53) pocket, an attempt to change the substitution pattern on the C6-aryl ring in **6** in order to adopt a different binding mode resulted in a great success (Figure 4). An in-house crystal structure of oxindole **2** (Figure 5b, transparent white) shows that the Leu26_(p53) pocket is filled by *m*-chlorophenyl group, which also makes a π - π stacking arrangement with His96 simultaneously. Since the oxindole **2** was one of the most potent MDM2 inhibitors at that time, we tried to induce a similar binding mode within the

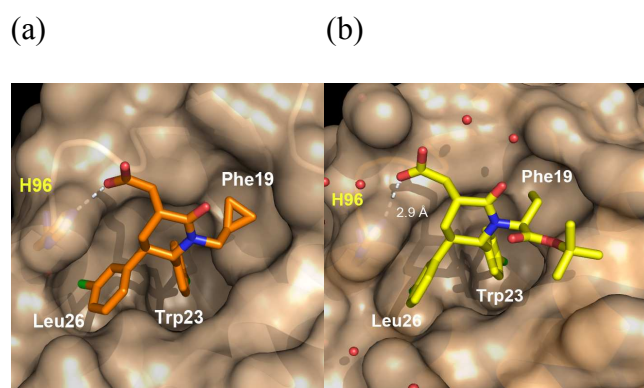
1
2
3 morpholinone chemotype. It was proposed that this reoriented binding mode could be induced by
4
5 shifting a halogen at the *para*-position in the C6 phenyl group of the morpholinone to the meta
6
7 position (**8** vs. **7** in Figure 4) so that the aromatic ring substitution pattern of this chemotype
8
9 would be identical to that of **2** (Figure 5b, cyan).
10
11
12
13
14
15
16



17
18
19
20
21
22
23
24
25
26
27
28
29 **Figure 5.** (a) X-ray co-crystal structure of the active isomer in **7** bound to MDM2 (cyan, PDB
30 4JV7). MDM2 binding pockets are labeled (by p53 side chain) in white. MDM2 residues are
31 labeled in yellow. Co-crystallized water molecules are depicted as red spheres.^{11b} (b) Model of
32 the morpholinone core (*N*-methyl, (*S*)-CH₃ at C2, cyan) in the proposed alternative binding mode
33 superimposed upon the co-crystal structure of **2** (transparent white, the electron density of the
34 pendant morpholinone is not fully resolved, PDB 4JVR).^{11b}
35
36
37
38
39
40
41
42
43
44
45

46 This hypothesis was soon verified by the SAR results of the synthesized compounds **8**–
47
48 **11** (Figure 4). Changing the halogen substitution of the C6 aryl from *para* to *meta* and the *N*-
49
50 alkyl group from methyl to cyclopropylmethyl led to compound **8**, showing a retained potency
51
52 relative to **7**. Incorporation of an acetic acid fragment at the C2 position resulted in a 6-fold
53
54 increase of potency (**9** vs. **8**). The improved potency can be rationalized by a strong electrostatic
55
56
57
58
59
60

1
2
3 interaction between the acetic acid functionality appended at C2 and the His96 residue of
4 MDM2, which is later observed in the co-crystal structure of **12** with MDM2. Notably, changing
5
6 MDM2, which is later observed in the co-crystal structure of **12** with MDM2. Notably, changing
7
8 the stereochemistry of the C6-aromatic ring was well tolerated within the morpholinone core (**10**
9
10 vs. **9**). Further modifications by inverting the stereochemical configuration of the acetic acid
11
12 substituent and switching the morpholinone core to a piperidinone, led to the identification of
13
14 *trans*-piperidinone lead **11** with improved potency.
15
16
17
18
19



33 **Figure 6.** (a) Model of proposed binding mode of piperidinone series lead **11**. MDM2 binding
34 pockets labeled (by p53 side chain) in white, H96 labeled in yellow.^{11a} (b) Co-crystal structure of
35 **12** bound to human MDM2 (17–111) at 1.8 Å resolution (yellow, PDB 4ERE). MDM2 binding
36 pockets labeled (by p53 side chain) in white, H96 labeled in yellow. Co-crystallized water
37 molecules are shown in red.^{11a}
38
39
40
41
42
43
44
45
46
47

48 The binding mode of **11** was predicted from docking studies. As shown in Figure 6a, it
49 was proposed that the C5 *m*-Cl phenyl group fills the Leu26_(p53) pocket, while the deepest
50 Trp23_(p53) pocket is occupied by the C6 *p*-Cl Phe group. The cyclopropylmethyl group occupies
51 the Phe19_(p53) pocket and the carboxylate anion forms an electrostatic interaction with the His96
52 imidazole side chain of MDM2. The binding mode of **11** was consistent with subsequent SAR
53
54
55
56
57
58
59
60

1
2
3 and confirmed by the co-crystal structure of its piperidinone analogue **12** (Figure 6b). Improved
4
5 potency of piperidinone **11** over morpholinones **9** and **10** was presumably due to the alleviation
6
7 of the electrostatically repulsive interaction between the carboxylic acid and the oxygen
8
9 embedded in the morpholinone ring by replacing the morpholinone core oxygen with a
10
11 methylene.
12
13
14
15
16

17 OPTIMIZATION OF PIPERIDINONE SERIES INHIBITORS VIA 18 19 CONFORMATIONAL CONTROLS AND EXTENSIVE SAR^{11a} 20 21

22 To maximize interaction with MDM2, the *N*-cyclopropylmethyl group in **11** requires a
23
24 downward orientation into the Phe19_(p53) pocket (Figure 6a and Figure 7). However, this *syn*
25
26 orientation shown in Figure 7 destabilizes the desired binding conformer. To stabilize the
27
28 conformation required to position the *N*-alkyl substituent into the Phe19_(p53) pocket, we decided
29
30 to introduce an additional hydrophilic substituent at the methylene adjacent to the ring nitrogen.
31
32 This exercise improved the binding affinity to MDM2 significantly by “directing” the highly
33
34 flexible *N*-substituent into the Phe19_(p53) pocket. Therefore, compound **12**, possessing a directing
35
36 group of *t*-butyl ester in the *N*-alkyl fragment, was 7–8 times more potent than **11** in both the
37
38 biochemical assay (IC₅₀ for **12** of 4.2 nM vs. IC₅₀ for **11** of 34 nM) and the cell proliferation
39
40 assay (IC₅₀ for **12** of 0.48 μM vs. IC₅₀ for **11** of 3.4 μM) (Figure 8). The co-crystal structure of
41
42 **12** bound to MDM2 confirms that the ethyl group reaches into the Phe19 (p53) pocket and the *t*-
43
44 butyl ester projects toward a solvent-exposed region. In addition, the C5 *m*-Cl phenyl group
45
46 engages in a face-to-face, π-stacking interaction with His96 while it fills the Leu26_(p53) pocket
47
48 (Figure 6b).
49
50
51
52
53
54
55
56
57
58
59
60

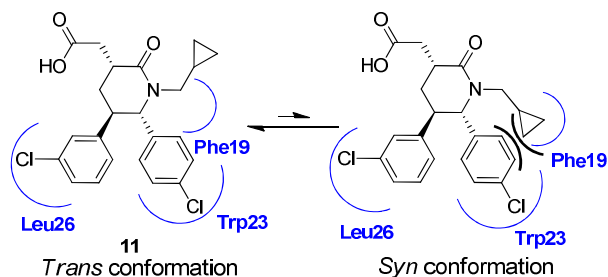


Figure 7. Interconversion of two cyclopropylmethyl conformations. MDM2 binding pockets are labeled (by p53 side chain) in blue.^{11a}

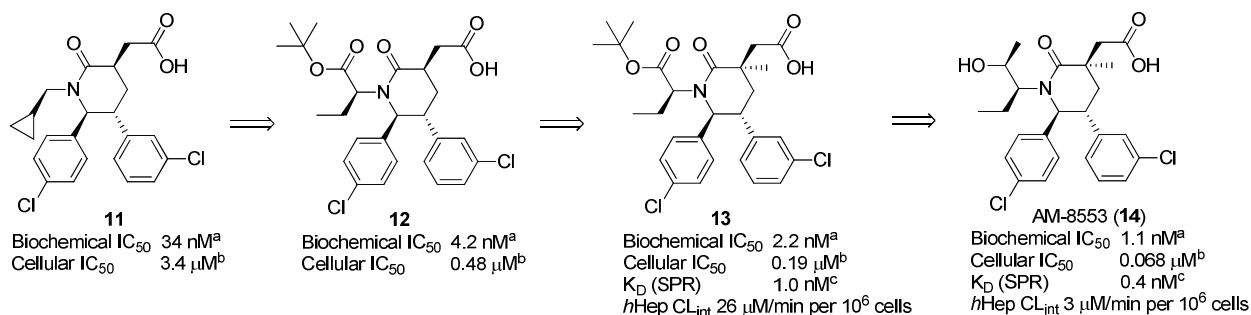
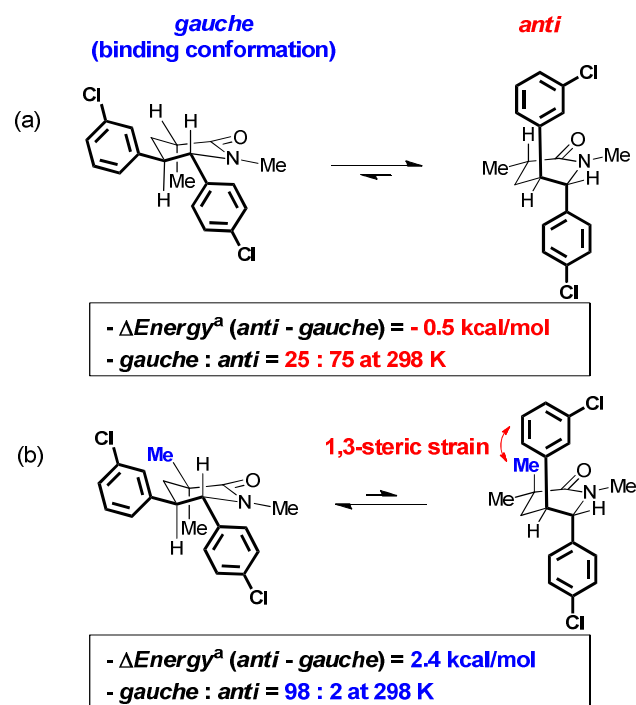


Figure 8. Optimization of potency and in vitro stability via a combination of conformational control and extensive SAR.^{11a} ^aIC₅₀ in the HTRF biochemical assay (serum free); ^bIC₅₀ in the EdU proliferation assay (SJSA-1, 10% human serum); ^cK_D in the SPR spectroscopy binding assay.



27 **Figure 9.** Conformers and relative energies (kcal/mol) for (a) C3 (*R*)-monosubstituted and (b)
 28 C3-disubstituted systems.^{11a} ^a Relative energy profile for *anti* and *gauche* conformations is
 29 calculated by the density functional theory (DFT) B3LYP/6-31g* method in Jaguar.^{11a}
 30
 31
 32
 33
 34
 35
 36

37 A closer look at the two aryl groups in the co-crystal structure of **12** indicates that the
 38 *trans*-C5 and C6 aryl groups have a *gauche*-like orientation in the presence of MDM2 (Figure
 39 6b). However, quantum mechanical calculations on the simple core structure (*N*-methyl, (*R*)-CH₃
 40 at C3; Figure 9a) suggest that in the free state, the more stable conformer instead possesses an
 41 *anti*-like orientation of the C5 and C6 aryls ($\Delta E = -0.5$ kcal/mol), which is less favorable for
 42 binding. On the other hand, incorporation of a methyl group at the C3 position substantially
 43 destabilizes the undesired *anti* conformation via a 1,3-steric interaction with the C5 aryl group,
 44 leading to a dominant *gauche* conformation (>98%; $\Delta E = 2.4$ kcal/mol, Figure 9b). This
 45 prediction translated well into potency increase of C3-methylated analogues.
 46
 47
 48
 49
 50
 51
 52
 53
 54
 55
 56
 57
 58
 59
 60

1
2
3
4
5
6
7
8
9
10
11
12
13
14
15
16
17
18
19
20
21
22
23
24
25
26
27
28
29
30
31
32
33
34
35
36
37
38
39
40
41
42
43
44
45
46
47
48
49
50
51
52
53
54
55
56
57
58
59
60

Compound **13** was approximately 2–3 times more potent than the corresponding C3 desmethyl analogue **12** in the HTRF biochemical assay (IC_{50} for **13** of 2.2 nM vs. IC_{50} for **12** of 4.2 nM) and the SJSA-1 proliferation assay (IC_{50} for **13** of 0.19 μ M vs. IC_{50} for **12** of 0.48 μ M) (Figure 8). The experimental conformational analysis of **12** and **13**, using the 1H NMR vicinal coupling constants between the C5 and C6 methine protons at two different temperatures, was also consistent with the theoretical predictions. Compound **13** was the first piperidinone inhibitor demonstrating a dose-dependent *in vivo* antitumor efficacy in the SJSA-1 osteosarcoma xenograft mouse model with an ED_{50} of 118 mg/kg.

Having identified a core structure with highly populated and well-defined free-state conformation suited for optimal binding, more efforts were made to further enhance potency and improve pharmacokinetic properties via optimization of the pendent *t*-butyl ester in **13**. As mentioned, the co-crystal structure of **12** strongly suggests that any replacement of the *t*-butyl ester group would project outward to the solvent region and not interact with MDM2. As predicted, a variety of functional groups is tolerated in this area. Replacing the *t*-butyl ester in **13** with a hydroxyethyl moiety produced the secondary alcohol **14** with high potency and low intrinsic clearance in human hepatocytes (Figure 8). In a SPR spectroscopy binding assay, the K_D for **14** and **13** was measured as 0.4 nM and 1.0 nM, respectively. Compound **14** was consistently more potent than **13** in the HTRF biochemical assay and the SJSA-1 cell proliferation assay as well (Figure 8). Compound **14** was also evaluated for its ability to inhibit tumor growth in the SJSA-1 xenograft mouse model. As expected, compound **14** significantly inhibited tumor growth at 150 and 200 mg/kg QD, compared to the vehicle, with an ED_{50} of 78 mg/kg. Compound **14** was found to have considerably reduced liability in the human pregnane X receptor (*h*PXR) assay, cytochrome P450 (CYP) inhibition assay, and time dependent inhibition (TDI) assay for

1
2
3 CYP3A4 isoform, as compared to **13**. The most significant improvement of **14** over **13** was its
4
5 projected human clearance (CL) (0.03 L/h/kg for **14** vs. 0.55 L/h/kg for **13**) along with a long
6
7 half-life (>12 h for **14** vs. 0.28 h for **13**), which resulted from greatly enhanced intrinsic
8
9 clearance in human hepatocytes (3.0 $\mu\text{L}/\text{min}$ per 10^6 cells for **14** vs. 26 $\mu\text{L}/\text{min}$ per 10^6 cells for
10
11 **13**).¹⁹ The co-crystal structure of **14** with MDM2 (Figure 10a) confirms that it occupies the three
12
13 critical binding pockets of MDM2 in a manner consistent with the previous co-crystal structure
14
15 of **12** (Figure 9b). Additionally, the C3 methyl group is found to have no direct interaction with
16
17 the protein and project toward the solvent, supporting our proposal that the potency increase
18
19 from C3 methylation (**13** vs. **12**) is conformationally induced and independent of protein
20
21 contacts.
22
23
24
25
26
27
28

29 **DISCOVERY OF **1** VIA CAPTURING AN ADDITIONAL INTERACTION WITH** 30 31 **GLY58 “SHELF” REGION**¹⁵ 32 33

34 Further analysis of the co-crystal structure of **14** suggests that exploration of a previously
35
36 underutilized region (G58 “shelf” region in Figure 10a) on the MDM2 surface might improve the
37
38 binding affinity of an inhibitor towards MDM2. When the secondary alcohol moiety in **14** was
39
40 replaced with a methyl sulfonamide, the resultant sulfonamide **15** had slightly improved
41
42 biochemical potency but weaker cellular potency (IC_{50} for **15** of 0.24 μM vs. IC_{50} for **14** of 0.068
43
44 μM), most likely due to the poor permeability (Figure 11). Interestingly, alignment of **15** to co-
45
46 crystal structures of **14** and related piperidinone inhibitors illustrates that the methyl moiety in
47
48 the sulfonamide side chain lies in the Gly58 “shelf” region bordered on the edge by F55, N59,
49
50 and M63 (Figure 10b).
51
52
53
54
55
56
57
58
59
60

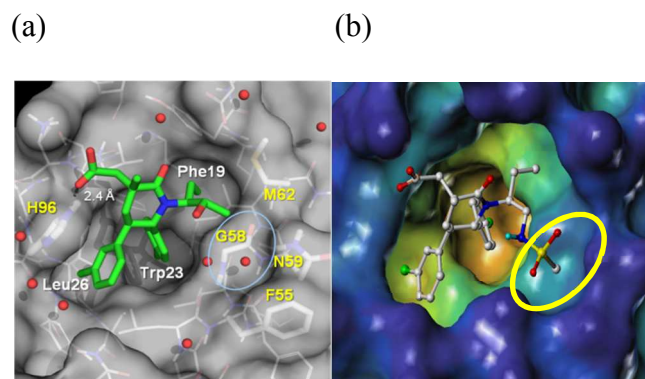


Figure 10. (a) Co-crystal structure of **14** bound to human MDM2 (17-111) at 2.0 Å resolution (green, PDB 4ERF) and depicting proposed electrostatic interaction with G58 “shelf” region (circled).^{11a, 15} MDM2 binding pockets labeled (by p53 side chain) in white. MDM2 residues, H96, G58, M62, N59, and F55 are labeled in yellow. Co-crystallized water molecules are shown in red. (b) Proposed binding mode of sulfonamide **15**.²⁰

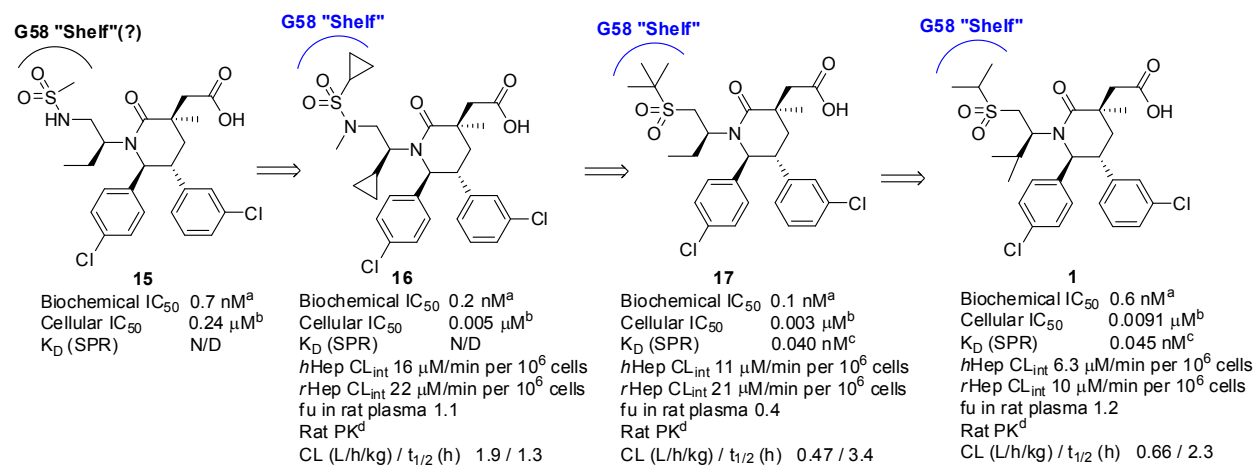


Figure 11. Discovery of **1** via identification and optimization of an additional interaction with Gly58 shelf region.¹⁵ ^aIC₅₀ in the HTRF biochemical assay (serum free); ^bIC₅₀ in the EdU proliferation assay (SJS-1, 10% human serum); ^cK_D in the SPR spectroscopy binding assay; ^dRat PK (iv, 0.5 mg/kg)

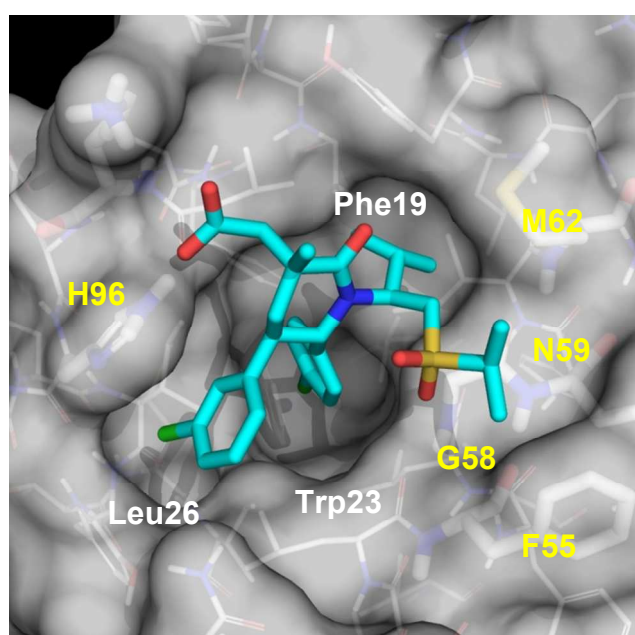
1
2
3
4
5
6
7
8
9
10
11
12
13
14
15
16
17
18
19
20
21
22
23
24
25
26
27
28
29
30
31
32
33
34
35
36
37
38
39
40
41
42
43
44
45
46
47
48
49
50
51
52
53
54
55
56
57
58
59
60

Once the interaction with this shallow predominantly hydrophobic cleft adjacent to the Phe19_(p53) pocket was optimized within the sulfonamide piperidinone series, we were able to discover highly potent MDM2 inhibitors such as the cyclopropyl sulfonamide **16** with single-digit nanomolar potency in cell proliferation assay (EdU IC₅₀ = 5.3 nM) (Figure 11). However, these sulfonamide inhibitors were found to have moderate to high in vivo clearance in rat and relatively high intrinsic clearance in human hepatocytes (i.e. 16 μL/min per 10⁶ cells for **16**), which was used for the human clearance prediction described below in the section of human PK prediction.¹⁹ Encouraged by the increased potency imparted by the sulfonamide functionality, we set out to explore the less polar and potentially more stable sulfone moiety to retain the favorable interaction with the glycine shelf and improve the metabolic stability. Gratifyingly, replacement of the sulfonamide group with a sulfone moiety provided a series of extremely potent MDM2 inhibitor exemplified as **17** in Figure 11. More importantly, many of these compounds maintain favorable cellular potency and have low intrinsic clearance in human hepatocytes and in vivo clearance in rat. Further optimization of *N*-alkyl substituent interacting with the Phe19_(p53) pocket led to the discovery of **1** (Figure 11). With its combination of high potency and excellent pharmacokinetics, compound **1** was chosen for further development.

BINDING MODE¹⁵

To understand specific interactions with MDM2, the binding mode of **1** was predicted from the co-crystal structures of **17** and related analogues (Figure 17).¹⁵ Compound **1** occupies the three critical binding pockets of Leu26_(p53), Trp23_(p53), and Phe19_(p53). The C5 aryl group fills the Leu26_(p53) pocket and engages in a face-to-face π-stacking interaction with His96, while the C6 aryl group reaches deep into the Trp23_(p53) binding cavity. The isopropyl group is directed

1
2
3 into the Phe19_(p53) pocket by the conformational constraint induced by the sulfone side chain.
4
5 The carboxylate functionality forms a strong hydrogen bond (2.7 Å) with the imidazole on the
6
7 His96 side chain of MDM2. In addition, the sulfone moiety properly projects the isopropyl group
8
9 to the glycine shelf region to maximize the hydrophobic contact with the neighboring proteins
10
11 while the sulfone itself is situated ca. 3.5 Å from the α -carbon of G58, suggesting a CH \cdots O type
12
13 interaction with this residue.
14
15
16
17
18
19



41
42 **Figure 12.** Binding mode of **1** based on the co-crystal structures of **17** bound to human MDM2
43
44 (17–111)(PDB code: 4OAS).¹⁵ MDM2 binding pockets are labeled (by p53 side chain) in white.
45
46 MDM2 residues H96, G58, M62, N59, and F55 are labeled in yellow.
47
48
49

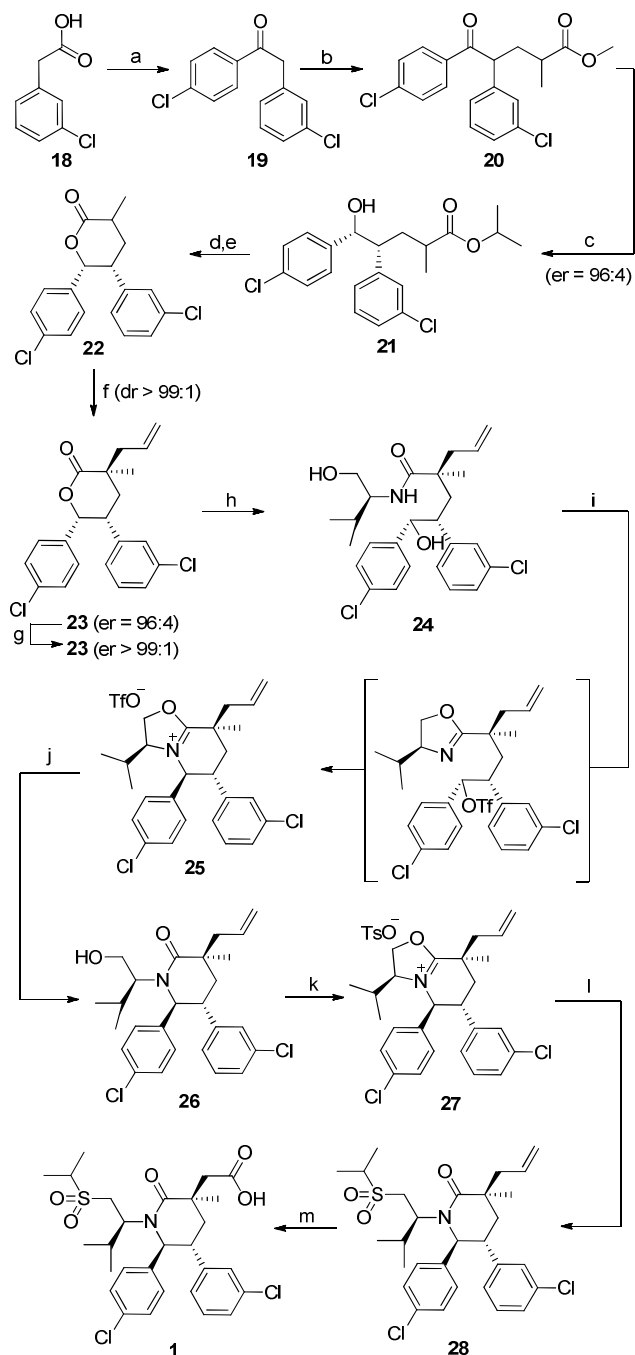
50
51
52 Furthermore, superimposition of the single crystal structure of **1** onto the co-crystal
53
54 structure of **17** shows that the binding conformation of **1** is essentially identical to the
55
56 conformation of **1** crystallized in the absence of protein. This suggests that **1** has the optimal
57
58
59
60

1
2
3 MDM2 binding with minimal conformational cost and the sulfone side chain is bound in the
4 extended low energy conformation. The favorable interactions and binding conformations of **17**
5
6 with MDM2 observed in the co-crystal structures greatly contribute to its high binding affinity
7
8 toward MDM2.
9
10

11 12 13 14 15 **CHEMICAL SYNTHESIS OF 1**^{15,21} 16

17
18 Asymmetric synthesis of **1** is described in Scheme 1. Overall, it was prepared in 12
19 linear steps beginning with 3-chlorophenylacetic acid **18**. Friedel-Crafts acylation of
20 chlorobenzene with the acid chloride of **18** gave ketone **19**. Conjugate addition of **19** to methyl
21 methacrylate provided keto ester **20** in 95% yield as a racemic mixture of diastereomers.
22
23 Catalytic hydrogenation of **20** in the presence of 0.4% RuCl₂[(*S*)-xyIBINAP][(*S*)-DAIPEN] with
24
25 40% sodium *tert*-butoxide in 2-propanol afforded compound **21** in 92% ee as a mixture of
26
27 diastereomers at C-2. This dynamic kinetic resolution is the key step in establishing the correct
28
29 absolute configuration of the piperidinone core of **1**.
30
31
32
33
34
35

36
37 The isopropyl ester of **21** was hydrolyzed to carboxylic acid with lithium hydroxide and
38
39 cyclized to lactone **22** in the presence of pyridinium *p*-toluenesulfonate (PPTS) under Dean-Stark
40
41 conditions in 81% overall yield from **20**. Lactone **22** was stereoselectively alkylated with allyl
42
43 bromide to afford the disubstituted lactone **23** in 94% yield with a diastereomeric ratio of greater
44
45 than 99:1. The enantiomeric excess of crystalline lactone **23** could be further improved to greater
46
47 than 98% by recrystallization from heptane.
48
49
50
51
52
53
54
55
56
57
58
59
60

Scheme 1.^a Asymmetric Synthesis of **1**

^a Reagents and conditions: (a) chlorobenzene, AlCl₃, SOCl₂, 89%; (b) methyl methacrylate, *t*-BuOK, THF, 95%; (c) 0.4% RuCl₂[(*S*)-xylBINAP][(S)-DAIPEN], *t*-BuONa, 2-propanol, H₂ (50 psi), 45 h; (d) LiOH, THF/MeOH/H₂O; (e) PPTS, toluene, reflux, 81% from **20**; (f) LiHMDS, allyl bromide, THF, -30 to -5 °C, 94%; (g) recrystallization from heptane, 80%; (h) L-Valinol, neat, 100 °C, 100%; (i) Tf₂O, lutidine, -50 °C; (j) LiOH, THF/H₂O then recrystallization from

1
2
3 cyclohexane, 75% from **24**; (k) TsOH, toluene, reflux, 100%; (l) 2-propanethiol, K₂CO₃, DMF,
4 50 °C, and then mCPBA, 0 °C, 90% over 2 steps; (m) RuCl₃, NaIO₄, EtOAc/CH₃CN/H₂O, then
5 recrystallization from EtOH/H₂O, 93%.
6
7
8
9

10 Addition of L-valinol to lactone **23** resulted in ring-opened amide **24** in quantitative yield,
11 and cyclization of **24** in the presence of trifluoromethanesulfonic anhydride gave intermediate
12 **25**. In this reaction, the triflate of the primary alcohol is rapidly displaced by the amide oxygen to
13 give an oxazoline ring. The nitrogen of the oxazoline then displaces the secondary triflate in a
14 S_N2-type fashion to give bicyclic oxazolinium triflate **25**. The subsequent basic hydrolysis of **25**
15 provided lactam **26** which was purified by column chromatography and recrystallization.
16
17
18
19
20
21
22
23

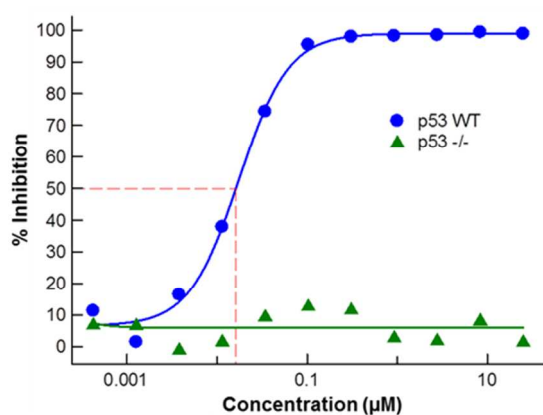
24 Acid-catalyzed cyclization of **26** resulted in the formation of oxazolinium tosylate **27**
25 which was opened with 2-propanethiol in the presence of lithium hydroxide. Oxidative workup
26 afforded sulfone **28** as the penultimate intermediate in 90% yield from **26**. Finally, ruthenium
27 chloride/sodium periodate oxidatively cleaved the terminal alkene to form the desired carboxylic
28 acid in 93% yield. Recrystallization from ethanol/water provided **1** with greater than 99%
29 chemical purity. This reliable and scalable route provided multi-hundred gram quantities of **1** for
30 its preclinical studies.
31
32
33
34
35
36
37
38
39
40
41
42

43 **IN VITRO AND IN VIVO PHARMACOLOGY**^{15,22}

44
45 Compound **1** significantly inhibits the human MDM2-p53 interaction in the biochemical
46 HTRF-based assay (IC₅₀ = 0.6 nM), but has no inhibition against MDMX at concentrations up to
47 10 μM. It binds to the human MDM2 in the SPR spectroscopy binding assay with a K_D of 0.045
48 nM. In the EdU proliferation assay, the molecule substantially suppresses growth of MDM2-
49 amplified SJSA-1 osteosarcoma tumor cells (IC₅₀ = 9.1 nM). Furthermore, compound **1** potently
50
51
52
53
54
55
56
57
58
59
60

1
2
3 inhibits proliferation of non-MDM2-amplified HCT116 colorectal cells in the BrdU assay (IC_{50}
4 = 10 nM).
5
6
7

8 The cellular selectivity of **1** was evaluated by examining its effect on the proliferation of
9 cultured HCT116 wild-type p53 ($p53^{wt}$) and p53-deficient ($p53^{-/-}$) tumor cells. As shown in
10 Figure 13, the molecule significantly inhibited the growth of wild-type p53 cells ($IC_{50} = 10$ nM)
11 in the BrdU proliferation assay, but had no growth inhibition of p53-deficient cells at
12 concentrations up to 10 μ M ($IC_{50} > 25$ μ M). The cellular selectivity between the deficient and
13 wild-type p53 lines was greater than 2500-fold, indicating that **1** has p53 dependent cell activity
14 exclusively.
15
16
17
18
19
20
21
22
23
24
25
26
27



38
39
40
41 **Figure 13.** Cell activity of **1** is p53 dependent. In HCT116 $p53^{wt}$ and $p53^{-/-}$ cells, the percentage
42 of BrdU positive cells was measured 16 h post-compound treatment by flow cytometry. DMSO
43 control was designated as 0% inhibition.
44
45
46
47
48
49
50
51

52 To understand the effect of **1** on p53 pathway signaling in vivo, we measured levels of
53 p21 mRNA induction, a transcriptional target and pharmacodynamic readout for p53 activity.²³
54
55 Treatment of SJSA-1 led to robust induction of p21 over 24 hours, with a peak p21 induction of
56
57
58
59
60

30-fold occurring at 4 hours post dose (Figure 14). This confirms that **1** effectively activates the p53 signaling in human tumors in vivo.

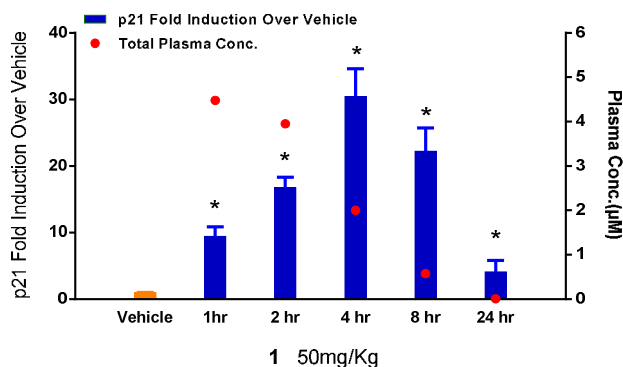


Figure 14. Pharmacodynamic study: treatment with **1** caused time and concentration dependent induction of p21 mRNA in SJSA-1 tumor xenografts. * $p < 0.05$. Female athymic nude mice were implanted subcutaneously with 5×10^6 SJSA-1 cells. When tumors reached $\sim 175 \text{ mm}^3$, 50 mg/kg of **1** or vehicle was administered orally once daily (QD) for 4 days. Mice were sacrificed on day 4 at 1, 2, 4, 8, and 24 hours post-dose ($n = 5/\text{group}$). Tumors were immediately removed and snap-frozen. p21 mRNA levels were measured by quantitative RT-PCR. Tumors treated with vehicle served as a negative control and indicated the baseline p21 mRNA level. Data are represented as mean p21 fold induction over vehicle and error bars represent SEM of data from five mice. Concentrations in plasma were analyzed by LC/MS/MS, and are plotted against the right y-axis.

To assess the ability of **1** to inhibit tumor growth in vivo, efficacy studies were performed in xenograft models of wild-type p53 human cancer cells. In the MDM2-amplified SJSA-1 osteosarcoma model, compound **1** displayed robust tumor growth inhibition compared to the

vehicle, with an ED₅₀ of 9.1 mg/kg QD (Figure 15). Unbound EC₅₀ associated with ED₅₀ was calculated as 2.8 nM.²⁴ Regression was observed with the two higher doses of 30 mg/kg and 60 mg/kg QD. The 60 mg/kg of dose caused complete tumor regression in 10 of 12 mice. No body weight loss was observed with any of the treatment groups.

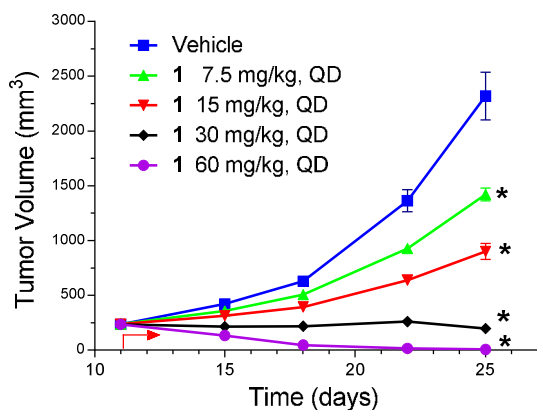


Figure 15. * $p < 0.05$. Treatment with **1** inhibited the growth of SJSA-1 tumors in vivo. SJSA-1 cells (5×10^6) were implanted subcutaneously into female athymic nude mice. Treatment with vehicle or **1** at 7.5, 15, 30 or 60 mg/kg QD by oral gavage began on day 11 when tumors had reached $\sim 200 \text{ mm}^3$ ($n=12/\text{group}$). Tumor sizes were measured twice per week. Data represent mean tumor volumes and the error bars represent SEM of data from 12 mice.

Compound **1** was also evaluated in the non-MDM2-amplified HCT-116 colorectal carcinoma xenograft model. Treatment with **1** twice a day dosing (BID) caused a dose-dependent tumor growth inhibition with an ED₅₀ of 16 mg/kg (Figure 16). The highest dose of 100 mg/kg BID resulted in tumor stasis (100% TDI) and no body weight loss was observed with any of the treatment groups. Tumor growth inhibition with QD dosing was comparable to that of BID dosing at all dose levels.²²

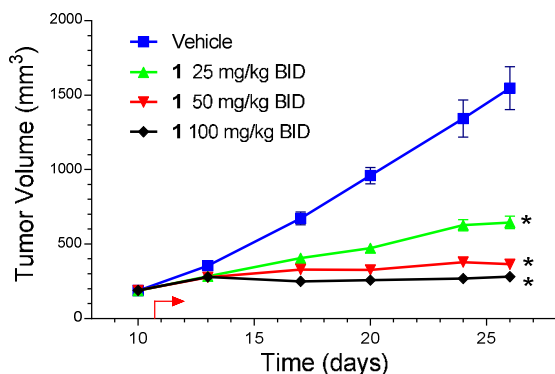


Figure 16. * $p < 0.0001$. Treatment with **1** inhibited the growth of HCT-116 tumors in vivo. HCT-116 colorectal carcinoma cells (5×10^6) were implanted subcutaneously into female athymic nude mice. Treatment with vehicle or **1** at 25, 50 or 100 mg/kg BID dosing by oral gavage began on day 11 when tumors had reached $\sim 200 \text{ mm}^3$ ($n=10/\text{group}$). Tumor sizes were measured twice per week. Data represent mean tumor volumes and the error bars represent SEM of data from 10 mice.

DRUG METABOLISM²⁵

The metabolism of **1** labeled with carbon-14 (Figure 17) was studied in hepatocytes from rat, dog, monkey, and human. Glucuronidation was found to be the primary metabolic pathway in hepatocytes from all species including human. The formation rate of acyl glucuronide (M1 in Figure 17) was determined to be in the order of dog > monkey > human > rat hepatocytes, which was consistent with the published data.²⁶ In an in vivo metabolism study, about 8% of administered dose was recovered as unchanged parent molecule in rat bile and feces over a period of 24 hours when [¹⁴C]-**1** was orally dosed in bile cannulated rats. In this study, acyl glucuronide was identified as a major metabolite along with two monohydroxyl metabolites. In

1
2
3
4
5
6
7
8
9
10
11
12
13
14
15
16
17
18
19
20
21
22
23
24
25
26
27
28
29
30
31
32
33
34
35
36
37
38
39
40
41
42
43
44
45
46
47
48
49
50
51
52
53
54
55
56
57
58
59
60

vitro and in vivo data suggest that metabolism is the major route of clearance and glucuronidation is the major metabolic pathway for **1**.

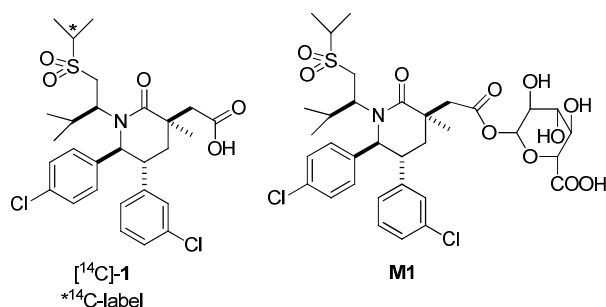


Figure 17. Structures of $[^{14}\text{C}]\text{-1}$ and major metabolite acyl glucuronide (M1).

PRECLINICAL PHARMACOKINETICS AND HUMAN PK PREDICTION²⁵

The preclinical pharmacokinetics of **1** were investigated in mouse, rat, cynomolgus monkey, and beagle dog following single-dose intravenous (IV) or oral administration. The molecule was found to have a low clearance and good oral bioavailability in mouse, rat and cynomolgus monkey, but high clearance and low oral bioavailability in beagle dog. Given the different pharmacokinetic properties of **1** in the preclinical species, in vitro–in vivo extrapolation of hepatocyte stability data¹⁹ was explored to predict the human clearance. As a result, good in vivo-in vitro correlation was observed in preclinical species when the hepatic intrinsic clearance values from preclinical species were scaled up to predict in vivo clearance. Using this method, **1** was predicted to have low clearance and a long half-life in humans.

SAFETY ASSESSMENT

1
2
3
4
5
6
7
8
9
10
11
12
13
14
15
16
17
18
19
20
21
22
23
24
25
26
27
28
Possible effects of **1** on enzyme activity and binding to receptors, were evaluated in the CEREP in vitro pharmacology assay panel. It was found to have no inhibition on any control specific binding at a concentration of 10 μM . In the ScanMax profiling assay, compound **1** was associated with only one hit out of 392 non-mutated kinases tested (protein kinase D2 (PRKD2), 69% inhibition at 10 μM). These data indicate that **1** is a highly selective inhibitor of MDM2. The cardiovascular safety profile of **1** was assessed through a combination of in vitro (hERG assay and isolated rabbit heart assay) and in vivo studies (rat telemetry study). These studies indicated no cardiovascular liability at exposure or concentration levels significantly higher than pharmacologically active exposures and concentrations. For example, in a single-dose rat cardiovascular telemetry study, no significant changes in cardiovascular variables were detected up to 250 mg/kg.

29
30
31
32
33
34
35
36
37
38
39
40
41
42
43
44
45
46
47
48
49
50
51
52
53
54
55
56
57
58
59
60
Compound **1** was a weak competitive inhibitor of CYP2C8 with an IC_{50} of 8.5 μM and not a potent inhibitor of CYP1A2, 2C9, 2C19, 2D6, 2E1 or 3A4, with IC_{50} of >30 μM , indicating low potential to affect clearance of co-administrated drugs by competitive inhibition of human CYP isoforms. PXR activation by **1** in vitro was evaluated using a PXR reporter gene assay. At 2 and 10 μM , **1** activated human PXR at 18 and 21% of positive control rifampicin at 10 μM , respectively. CYP induction assay was carried out with human hepatocytes from donors, the changes in mRNA level and activity of CYP3A4, CYP2B6, and CYP1A2 were minor at 1 μM of **1**. Overall potential for **1** to increase clearance of CYP3A4 substrates is considered low due to the relatively low exposure at a projected clinically efficacious dose. In vivo nonclinical toxicology profile of **1** was evaluated in the preclinical species where no safety findings precluded progression of **1** to clinical development.

CONCLUSION

Combination of de novo design, X-ray crystallography, molecular modeling, and iterative medicinal chemistry, resulted in the discovery of piperidinone MDM2 inhibitors. Further optimization of this series through conformational controls, extensive SAR studies, and capturing an additional interaction with Gly58 “shelf” region led to the discovery of **1**, which is a highly potent MDM2 inhibitor in clinical trials. Compound **1** has favorable in vitro and in vivo toxicology profiles. Moreover, this molecule is projected to have low clearance and a long half-life in humans.

AUTHOR INFORMATION

Corresponding Authors

* Y.R.: (address) 1120 Veterans Blvd., South San Francisco, CA 94080; (phone, office) 650-244-2682; (e-mail) yrew@amgen.com

* D.S.: (address) 1120 Veterans Blvd., South San Francisco, CA 94080; (phone, office) 650-244-2195; (e-mail) daqings@amgen.com

ABBREVIATIONS USED

BID, twice a day dosing; BrdU, 5-bromo-2-deoxyuridine; CL, clearance; CYP, Cytochrome P450; DMF, *N,N*-dimethylformamide; DMSO, dimethylsulfoxide; dr, diastereoselectivity ratio; EC₅₀, half maximal effective concentration; ED₅₀, median effective dose; EdU, 5-ethynyl-2'-deoxyuridine; ee, enantiomeric excess; er, enantioselectivity ratio; EtOAc, ethyl acetate; EtOH, ethanol; *fu*, fraction unbound; *h*PXR, Human Pregnane X Receptor; HTRF, homogeneous time-resolved fluorescence; HTS, High-throughput screening; IC₅₀, half maximal inhibitory

1
2
3 concentration; IV, intravenous; LiHMDS, lithium bis(trimethylsilyl)amide; MeOH, Methanol;
4
5 MDM2, murine double minute 2; NMR, Nuclear magnetic resonance; PPTS, pyridinium *p*-
6
7 toluenesulfonate; PK, pharmacokinetics; PXR, pregnane X receptor; QD, once a day dosing; RT-
8
9 PCR, reverse transcription polymerase chain reaction; SAR, structure activity relationship; SEM,
10
11 standard error of mean; SN2, substitution nucleophilic (bi-molecular); SPR, Surface Plasmon
12
13 Resonance; *t*-BuOK, potassium *tert*-butoxide; *t*-BuONa, sodium *tert*-butoxide; TDI, time
14
15 dependent inhibition; Tf₂O, Trifluoromethanesulfonic anhydride; THF, tetrahydrofuran; TsOH,
16
17 4-toluenesulfonic acid.
18
19
20
21
22
23
24
25

26 REFERENCES

- 27
28
29 (1) Vazquez, A.; Bond, E. E.; Levine, A. J.; Bond, G. L., The genetics of the p53 pathway,
30
31 apoptosis and cancer therapy. *Nat. Rev. Drug Discovery* **2008**, *7*, 979-987.
32
33
34 (2) Vogelstein, B.; Lane, D.; Levine, A. J., Surfing the p53 network. *Nature (London)* **2000**, *408*,
35
36 307-310.
37
38
39 (3) (a) Hollstein, M.; Sidransky, D.; Vogelstein, B.; Harris, C. C., p53 Mutations in human
40
41 cancers. *Science (Washington, D.C.)* **1991**, *253*, 49-53; (b) Soussi, T.; Dehouche, K.; Beroud, C.,
42
43 p53 Web-site and analysis of p53 gene mutations in human cancer: forging a link between
44
45 p53 Web-site and analysis of p53 gene mutations in human cancer: forging a link between
46
47 epidemiology and carcinogenesis. *Hum. Mutat.* **2000**, *15*, 105-113.
48
49
50 (4) (a) Chene, P., Inhibiting the p53-MDM2 interaction: An important target for cancer therapy.
51
52 *Nature Rev. Cancer* **2003**, *3*, 102-109; (b) Oliner, J. D.; Kinzler, K. W.; Meltzer, P. S.; George,
53
54
55
56
57
58
59
60

1
2
3 D. L.; Vogelstein, B., Amplification of a gene encoding a p53-associated protein in human
4 sarcomas. *Nature (London)* **1992**, *358*, 80-83.
5
6

7
8
9 (5) (a) Momand, J.; Zambetti, G. P.; Olson, D. C.; George, D.; Levine, A. J., The MDM-2
10 oncogene product forms a complex with the p53 protein and inhibits p53-mediated
11 transactivation. *Cell* **1992**, *69*, 1237-1245; (b) Oliner, J. D.; Pietenpol, J. A.; Thiagalingam, S.;
12 Gyuris, J.; Kinzler, K. W.; Vogelstein, B., Oncoprotein MDM2 conceals the activation domain
13 of tumor suppressor p53. *Nature (London)* **1993**, *362*, 857-860.
14
15
16
17
18
19

20
21 (6) (a) Roth, J.; Dobbstein, M.; Freedman, D. A.; Shenk, T.; Levine, A. J., Nucleo-cytoplasmic
22 shuttling of the hdm2 oncoprotein regulates the levels of the p53 protein via a pathway used by
23 the human immunodeficiency virus rev protein. *EMBO J.* **1998**, *17*, 554-564; (b) Tao, W.;
24 Levine, A. J., Nucleocytoplasmic shuttling of oncoprotein Hdm2 is required for Hdm2-mediated
25 degradation of p53. *Proc. Natl. Acad. Sci. U.S.A.* **1999**, *96*, 3077-3080.
26
27
28
29
30
31
32

33
34 (7) (a) Haupt, Y.; Maya, R.; Kazaz, A.; Oren, M., MDM2 promotes the rapid degradation of p53.
35 *Nature (London)* **1997**, *387*, 296-299; (b) Kubbutat, M. H. G.; Vousden, k. H., Proteolytic
36 cleavage of human p53 by calpain: a potential regulator of protein stability. *Mol. Cell. Biol.*
37 **1997**, *17*, 460-468.
38
39
40
41
42
43
44

45 (8) Vassilev, L. T., MDM2 inhibitors for cancer therapy. *Trends Mol. Med.* **2007**, *13*, 23-31.
46
47

48 (9) (a) Vassilev, L. T.; Vu, B. T.; Graves, B.; Carvajal, D.; Podlaski, F.; Filipovic, Z.; Kong, N.;
49 Kammlott, U.; Lukacs, C.; Klein, C.; Fotouhi, N.; Liu, E. A., In vivo activation of the p53
50 pathway by small-molecule antagonists of MDM2. *Science (Washington, D.C.)* **2004**, *303*, 844-
51 848; (b) Tovar, C.; Rosinski, J.; Filipovic, Z.; Higgins, B.; Kolinsky, K.; Hilton, H.; Zhao, X.;
52
53
54
55
56
57
58
59
60

Vu, B. T.; Qing, W.; Packman, K.; Myklebost, O.; Heimbrook, D. C.; Vassilev, L. T., Small-molecule MDM2 antagonists reveal aberrant p53 signaling in cancer: implications for therapy. *Proc. Natl. Acad. Sci. U.S.A.* **2006**, *103*, 1888-1893.

(10) (a) Ding, K.; Lu, Y.; Nikolovska-Coleska, Z.; Qiu, S.; Ding, Y.; Gao, W.; Stuckey, J.; Krajewski, K.; Roller, P. P.; Tomita, Y.; Parrish, D. A.; Deschamps, J. R.; Wang, S., Structure-based design of potent non-peptide MDM2 inhibitors. *J. Am. Chem. Soc.* **2005**, *127*, 10130-10131; (b) Ding, K.; Lu, Y.; Nikolovska-Coleska, Z.; Wang, G.; Qiu, S.; Shangary, S.; Gao, W.; Qin, D.; Stuckey, J.; Krajewski, K.; Roller, P. P.; Wang, S., Structure-based design of spirooxindoles as potent, specific small-molecule inhibitors of the MDM2-p53 interaction. *J. Med. Chem.* **2006**, *49*, 3432-3435; (c) Shangary, S.; Qin, D.; McEachern, D.; Liu, M.; Miller, R. S.; Qiu, S.; Nikolovska-Coleska, Z.; Ding, K.; Wang, G.; Chen, J.; Bernard, D.; Zhang, J.; Lu, Y.; Gu, Q.; Shah, R. B.; Pienta, K. J.; Ling, X.; Kang, S.; Guo, M.; Sun, Y.; Yang, D.; Wang, S., Temporal activation of p53 by a specific MDM2 inhibitor is selectively toxic to tumors and leads to complete tumor growth inhibition. *Proc. Natl. Acad. Sci. U.S.A.* **2008**, *105*, 3933-3938; (d) Yu, S.; Qin, D.; Shangary, S.; Chen, J.; Wang, G.; Ding, K.; McEachern, D.; Qiu, S.; Nikolovska-Coleska, Z.; Miller, R.; Kang, S.; Yang, D.; Wang, S., Potent and orally active small-molecule inhibitors of the MDM2-p53 interaction. *J. Med. Chem.* **2009**, *52*, 7970-7973.

(11) (a) Rew, Y.; Sun, D.; Gonzalez-Lopez De Turiso, F.; Bartberger, M. D.; Beck, H. P.; Canon, J.; Chen, A.; Chow, D.; Deignan, J.; Fox, B. M.; Gustin, D.; Huang, X.; Jiang, M.; Jiao, X.; Jin, L.; Kayser, F.; Kopecky, D. J.; Li, Y.; Lo, M.-C.; Long, A. M.; Michelsen, K.; Oliner, J. D.; Osgood, T.; Ragains, M.; Saiki, A. Y.; Schneider, S.; Toteva, M.; Yakowec, P.; Yan, X.; Ye, Q.; Yu, D.; Zhao, X.; Zhou, J.; Medina, J. C.; Olson, S. H., Structure-based design of novel inhibitors of the MDM2-p53 interaction. *J. Med. Chem.* **2012**, *55*, 4936-4954; (b) Gonzalez-

1
2
3 Lopez de Turiso, F.; Sun, D.; Rew, Y.; Bartberger, M. D.; Beck, H. P.; Canon, J.; Chen, A.;
4
5 Chow, D.; Correll, T. L.; Huang, X.; Julian, L. D.; Kayser, F.; Lo, M.-C.; Long, A. M.; McMinn,
6
7 D.; Oliner, J. D.; Osgood, T.; Powers, J. P.; Saiki, A. Y.; Schneider, S.; Shaffer, P.; Xiao, S.-H.;
8
9 Yakowec, P.; Yan, X.; Ye, Q.; Yu, D.; Zhao, X.; Zhou, J.; Medina, J. C.; Olson, S. H., Rational
10
11 design and binding mode duality of MDM2-p53 inhibitors. *J. Med. Chem.* **2013**, *56*, 4053-4070.
12
13

14
15
16 (12) Zhao, Y.; Yu, S.; Sun, W.; Liu, L.; Lu, J.; McEachern, D.; Shargary, S.; Bernard, D.; Li, X.;
17
18 Zhao, T.; Zou, P.; Sun, D.; Wang, S., A potent small-molecule inhibitor of the MDM2-p53
19
20 interaction (MI-888) achieved complete and durable tumor regression in mice. *J. Med. Chem.*
21
22 **2013**, *56*, 5553-5561.
23
24

25
26 (13) (a) Vu, B.; Wovkulich, P.; Pizzolato, G.; Lovey, A.; Ding, Q.; Jiang, N.; Liu, J.-J.; Zhao, C.;
27
28 Glenn, K.; Wen, Y.; Tovar, C.; Packman, K.; Vassilev, L.; Graves, B., Discovery of RG7112: A
29
30 small-molecule MDM2 inhibitor in clinical development. *ACS Med. Chem. Lett.* **2013**, *4*, 466-
31
32 469; (b) Ding, Q.; Zhang, Z.; Liu, J.-J.; Jiang, N.; Zhang, J.; Ross, T. M.; Chu, X.-J.; Bartkovitz,
33
34 D.; Podlaski, F.; Janson, C.; Tovar, C.; Filipovic, Z. M.; Higgins, B.; Glenn, K.; Packman, K.;
35
36 Vassilev, L. T.; Graves, B., Discovery of RG7388, a potent and selective p53-MDM2 inhibitor in
37
38 clinical development. *J. Med. Chem.* **2013**, *56*, 5979-5983; (c) Zhang, Z.; Chu, X.-J.; Liu, J.-J.;
39
40 Ding, Q.; Zhang, J.; Bartkovitz, D.; Jiang, N.; Karnachi, P.; So, S.-S.; Tovar, C.; Filipovic, Z.
41
42 M.; Higgins, B.; Glenn, K.; Packman, K.; Vassilev, L.; Graves, B., Discovery of potent and
43
44 orally active p53-MDM2 inhibitors RO5353 and RO2468 for potential clinical development.
45
46 *ACS Med. Chem. Lett.* **2014**, *5*, 124-127.
47
48
49
50
51

52
53 (14) Carry, J.-C.; Garcia-Echeverria, C., Inhibitors of the p53/hdm2 protein-protein interaction-
54
55 path to the clinic. *Bioorg. Med. Chem. Lett.* **2013**, *23*, 2480-2485.
56
57
58
59
60

1
2
3 (15) Sun, D.; Li, Z.; Rew, Y.; Gribble, M.; Bartberger, M. D.; Beck, H. P.; Canon, J.; Chen, A.;
4
5 Chen, X.; Chow, D.; Deignan, J.; Duquette, J.; Eksterowicz, J.; Fisher, B.; Fox, B. M.; Fu, J.;
6
7 Gonzalez, A. Z.; Gonzalez Lopez De Turiso, F.; Houze, J.; Huang, X.; Jiang, M.; Jin, L.; Kayser,
8
9 F.; Liu, J. J.; Lo, M.-C.; Long, A. M.; Lucas, B.; McGee, L. R.; McIntosh, J.; Mihalic, J.; Oliner,
10
11 J. D.; Osgood, T.; Peterson, M. L.; Roveto, P.; Saiki, A. Y.; Shaffer, P.; Toteva, M.; Wang, Y.;
12
13 Wang, Y. C.; Wortman, S.; Yakowec, P.; Yan, X.; Ye, Q.; Yu, D.; Yu, M.; Zhao, X.; Zhou, J.;
14
15 Zhu, J.; Olson, S. H.; Medina, J. C., Discovery of AMG 232, a potent, selective, and orally
16
17 bioavailable inhibitor of the MDM2-p53 interaction in clinical development. *J. Med. Chem.*
18
19 **2014**, *57*, 1454-1472.
20
21
22
23
24

25 (16) (a) Allen, J. G.; Bourbeau, M. P.; Wohlhieter, G. E.; Bartberger, M. D.; Michelsen, K.;
26
27 Hungate, R.; Gadwood, R. C.; Gaston, R. D.; Evans, B.; Mann, L. W.; Matison, M. E.;
28
29 Schneider, S.; Huang, X.; Yu, D.; Andrews, P. S.; Reichelt, A.; Long, A. M.; Yakowec, P.;
30
31 Yang, E. Y.; Lee, T. A.; Oliner, J. D., Discovery and optimization of
32
33 chromenotriazolopyrimidines as potent inhibitors of the mouse double minute 2-tumor protein 53
34
35 protein-protein interaction. *J. Med. Chem.* **2009**, *52*, 7044-7053; (b) Beck, H. P.; DeGraffenreid,
36
37 M.; Fox, B.; Allen, J. G.; Rew, Y.; Schneider, S.; Saiki, A. Y.; Yu, D.; Oliner, J. D.; Salyers, K.;
38
39 Ye, Q.; Olson, S., Improvement of the synthesis and pharmacokinetic properties of
40
41 chromenotriazolopyrimidine MDM2-p53 protein-protein inhibitors. *Bioorg. Med. Chem. Lett.*
42
43 **2011**, *21*, 2752-2755.
44
45
46
47
48
49

50 (17) Kussie, P. H.; Gorina, S.; Marechal, V.; Elenbaas, B.; Moreau, J.; Levine, A. J.; Pavletich,
51
52 N. P., Structure of the MDM2 oncoprotein bound to the p53 tumor suppressor transactivation
53
54 domain. *Science (Washington, D.C.)* **1996**, *274*, 948-953.
55
56
57
58
59
60

1
2
3 (18) Oxindole **2** is a diastereomer of MI-63 reported by Wang and co-workers (See ref. (10) (b)
4 Ding et, JMC, 2006). The stereochemistry and binding mode of inhibitor **2** were determined
5
6 from in-house co-crystal structure (See ref. (11) (b) Gonzalez-Lopez de Turiso et al, JMC, 2013).
7
8

9
10
11 (19) Ye, Q.; Jiang, B. M.; Chan, H.; Wong, K. B.; Jin, L., Optimization of hepatocyte intrinsic
12 clearance assay for human metabolic clearance prediction: impact of assay conditions on
13 prediction accuracy. Unpublished results.
14
15
16

17
18
19 (20) Details of the story about how to discover the “Gly58 Self” region in MDM2 to boost
20 binding affinity of MDM2 inhibitors will be reported in due course.
21
22

23
24 (21) Lucas, B. S.; Fisher, B.; McGee, L. R.; Olson, S. H.; Medina, J. C.; Cheung, E., An
25 expeditious synthesis of the MDM2-p53 inhibitor AM-8553. *J. Am. Chem. Soc.* **2012**, *134*,
26 12855-12860.
27
28
29

30
31
32 (22) Canon, J.; Osgood, T.; Olson, S.; Saiki, A.; Robertson, R.; Bartberger, M.; Sun, D.; Ye, Q.;
33 Jin, L.; Yu, D.; Ada Chen, A.; Zhou, J.; Cordover, D.; Kaufman, S.; Oliner, J.; Coxon, A.;
34 Radinsky, R., The MDM2 inhibitor AMG 232 demonstrates robust anti-tumor activity and
35 potentiates the activity of p53-inducing cytotoxic agents. Unpublished results.
36
37
38

39
40
41 (23) El-Deiry, W. S.; Tokino, T.; Velculescu, V. E.; Levy, D. B.; Parsons, R.; Trent, J. M.; Lin,
42 D.; Mercer, W. E.; Kinzler, K. W.; Vogelstein, B., WAF1, a potential mediator of p53 tumor
43 suppression. *Cell* **1993**, *75*, 817-825.
44
45
46
47

48
49
50 (24) Details of the study will be reported in due course.
51
52

53
54 (25) Ye, Q.; Jiang, M.; Huang, W. T.; Ling, Y.; Olson, S. H.; Sun, D.; Xu, G.; Yan, X.; Jin, L.,
55 Pharmacokinetics and metabolism of AMG 232, a novel and orally bioavailable inhibitor of the
56
57
58
59
60

1
2
3 MDM2–p53 interaction, in rat, dog, and monkey: in vitro-in vivo correlation. Unpublished
4
5 results.
6
7

8
9 (26) Wen, Z.; Martin, D. E.; Bullock, P.; Lee, K.-H.; Smith, P. C., Glucuronidation of anti-HIV
10
11 drug candidate bevirimat: identification of human UDP-glucuronosyltransferases and species
12
13 differences. *Drug Metab. Dispos.* **2007**, 35, 440-448.
14
15
16
17
18
19
20
21
22
23
24
25
26
27
28
29
30
31
32
33
34
35
36
37
38
39
40
41
42
43
44
45
46
47
48
49
50
51
52
53
54
55
56
57
58
59
60

1
2
3 For Table of Contents Only
4
5
6
7

